Electronic Supplementary Information (ESI)

An integrated approach (synthetic, structural and biological) in the study of aroylhydrazone salts

Višnja Vrdoljak, Biserka Prugovečki, Ines Primožič, Tomica Hrenar, Danijela Cvijanović, Jelena Parlov Vuković, Renata Odžak, Mirjana Skočibušić, Stjepan Prugovečki, Jasna Lovrić, Dubravka Matković-Čalogović, Marina Cindrić

Contents

1. Powder X-ray diffraction patterns

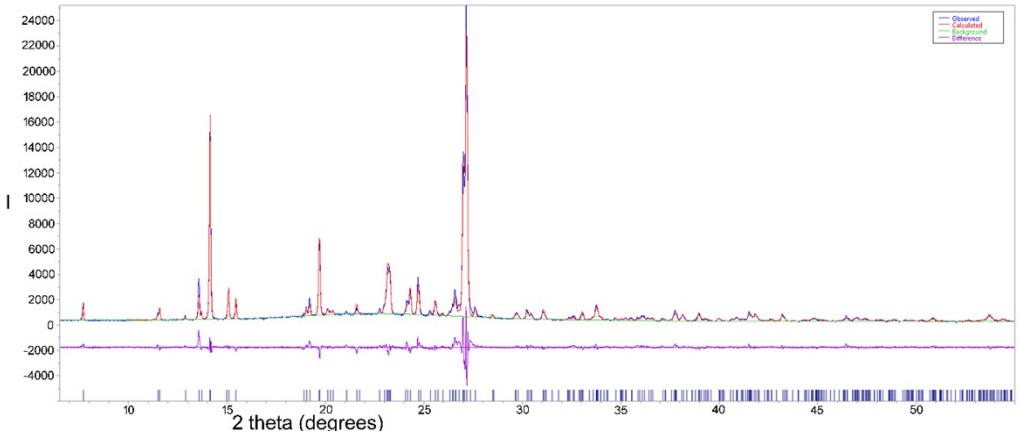

(a)

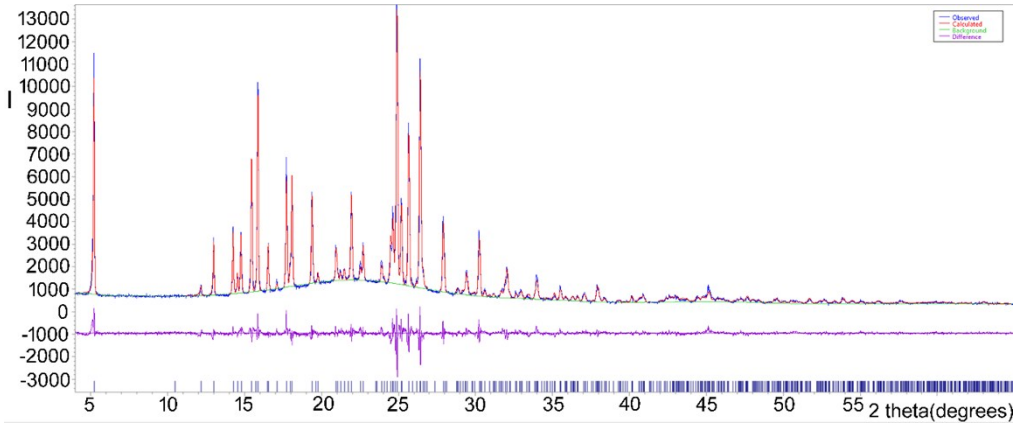

(b)

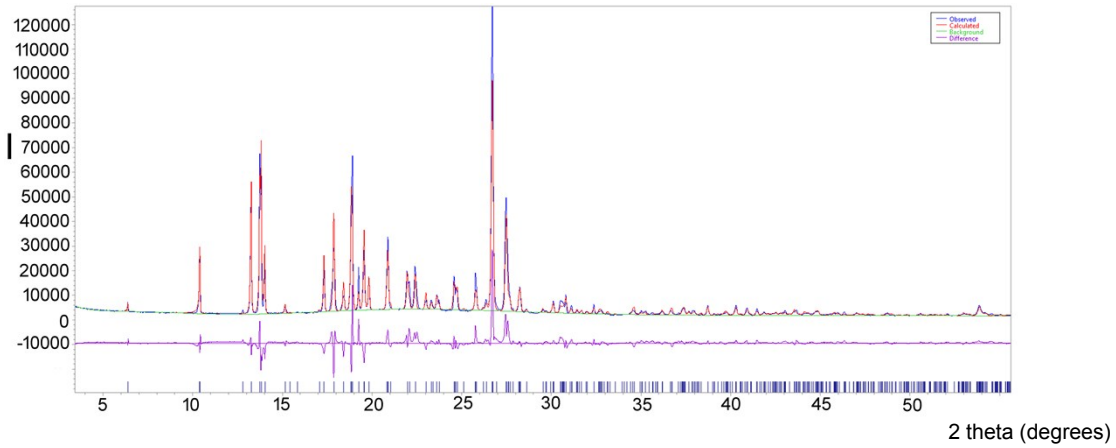

(c)

Figure S1. (a) The final Rietveld plot of $(HL^1)^+NO_3^-$ (R_p = 0.07580, R_{wp} = 0.0847).; (**b**) The final Rietveld plot of $(HL^1)^+HSO_4^-$ (**α**). (R_p = 0.0515, R_{wp} = 0.0672). (**c**) The final Rietveld plot of $(HL^1)^+HSO_4^-$ (**β**). (R_p = 0.0953, R_{wp} = 0.1363). Blue-observed pattern, red-calculated, green-background, magenta-difference.

2. *Synthesis, analytical data and disolution rate*

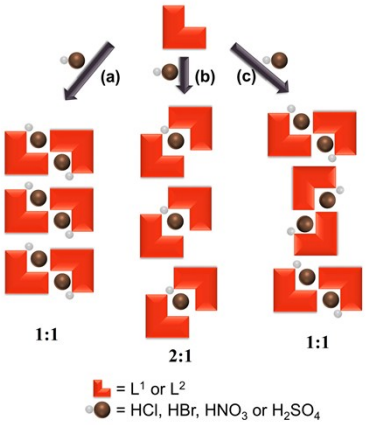

Scheme S1. Schematic representation of the possible solid-state forms (2:1 salt and different polymorphic forms of 1:1 salt). When an acid was added at 10-15 °C to the solution the conditions were as follows: (a) the reaction mixture was stirred for 1 h; (b) the solution was stirred at 25 °C for 1 h and then at 40 °C for 3 h, after which it was evaporated slowly for a few days; (c) the same procedure as described under (b) only that the solution was evaporated under vacuum.

$(HL^1)^+Cl^-$. Anal. Calcd. for $C_{14}H_{14}ClN_3O_3$ (307.732): C, 54.64; H, 4.59; N, 13.65. Found: C, 54.43; H, 4.61; N, 13.38%. DSC melting peak: onset 201.0 °C. Selected IR data (cm^{-1}): 1684 (C=O), 1625 (ring C=C), 1597 (ring C=C), 1554 (N=CH), 1501 (NN–H), 1439 (C–OH), 1279 ($C–OCH_3$).

$(HL^1)^+Br^-$ (α). Anal. Calcd. for $C_{14}H_{14}BrN_3O_3$ (352.183): C, 47.74; H, 4.01; N, 11.93. Found: C, 47.56; H, 4.21; N, 11.66%. DSC melting peak: onset 241.0 °C. Selected IR data (cm^{-1}): 1682 (C=O), 1624 (ring C=C), 1597 (ring C=C), 1539 (N=CH), 1491 (NN–H), 1440 (C–OH), 1273 ($C–OCH_3$).

$(HL^1)^+Br^-$ (β). Anal. Calcd. for $C_{14}H_{14}BrN_3O_3$ (352.183): C, 47.74; H, 4.01; N, 11.93. Found: C, 47.63; H, 4.17; N, 11.73%. DSC melting peak: onset 244.0 °C. Selected IR data (cm^{-1}): from 2625 to 2279 (N–H intermolecular), 1686 (C=O), 1626 (ring C=C), 1595 (ring C=C), 1548 (N=CH), 1498 (NN–H), 1442 (C–OH), 1274 ($C–OCH_3$).

$[H(L^1)_2]^+Br^-$. Anal. Calcd. for $C_{14}H_{14}BrN_3O_3$ (623.454): C, 53.94; H, 4.37; N, 13.48. Found: C, 54.71; H, 4.11; N, 13.25 %. DSC melting peak: onset 247.0 °C. Selected IR data (cm^{-1}): 1682 (C=O), 1628 (ring C=C), 1606 (ring C=C), 1540 (N=CH), 1500 (NN–H), 1441 (C–OH), 1270 ($C–OCH_3$).

$(HL^1)^+NO_3^-$. Anal. Calcd. for $C_{14}H_{14}N_4O_6$ (334.2843): C, 50.30; H, 4.22; N, 16.76. Found: C, 50.18; H, 3.99; N, 16.57%. DSC: onset 198.0 °C. Selected IR data (cm^{-1}): 1677 (C=O), 1625 (ring C=C), 1600 (ring C=C), 1556 (N=CH), 1500 (NN–H), 1440 (C–OH), 1276 ($C–OCH_3$).

$(HL^1)^+HSO_4^-$ (α).[1] Anal. Calcd. for $C_{14}H_{15}N_3O_7S$ (369.350): C, 45.53; H, 4.09; N, 11.38. Found: C, 45.56; H, 3.76; N, 11.66%. DSC melting peak: onset 213.0 °C. Selected IR data (cm^{-1}): 1678 (C=O), 1628 (ring C=C), 1599 (ring C=C), 1551 (N=CH), 1500 (NN–H), 1442 (C–OH), 1277 (C–OCH_3).

$(HL^1)_2^{2+}SO_4^{2-}$.[1] Yield: 0.07 g; 66 %. Anal. Calcd. for $C_{28}H_{28}N_6O_{10}S$ (640.62): C, 52.50; H, 4.41; N, 13.12. Found: C, 52.33; H, 4.21; N, 12.95%. DSC melting peak: onset 229.0 °C. Selected IR data (cm^{-1}): 1668 (C=O), 1626 (ring C=C), 1599 (ring C=C), 1566 (N=CH), 1492 (NN–H), 1441 (C–OH), 1284 (C–OCH_3).

$(HL^1)^+HSO_4^-$ (β).[1] Anal. Calcd. for $C_{14}H_{15}N_3O_7S$ (369.350): C, 45.53; H, 4.09; N, 11.38. Found: C, 45.38; H, 3.6; N, 11.52%. DSC melting peak: onset 189.0 °C. Selected IR data (cm^{-1}): 1678 (C=O), 1622 (ring C=C), 1602 (ring C=C), 1556 (N=CH), 1498 (NN–H), 1450 (C–OH), 1276 (C–OCH_3).

$(HL^2)^+Cl^-\cdot 0.5H_2O$. Anal. Calcd. for $C_{14}H_{15}ClN_3O_{3.5}$ (316.740): C, 53.09; H, 4.77; N, 13.27. Found: C, 52.80; H, 4.66; N, 13.08%. DSC melting peak: onset 186.0 °C. Selected IR data (cm^{-1}): 1687 (C=O), 1621 (ring C=C), 1604 (ring C=C), 1576 (N=CH), 1500 (NN–H), 1476 (ring C–H bending), 1373 (–OH bending), 1245 (C–OCH_3).

$(HL^2)^+Br^-\cdot MeOH$. Anal. Calcd. for $C_{14}H_{13}BrN_3O_3$ (352.183): C, 47.74; H, 4.01; N, 11.93. Found: C, 47.63; H, 4.17; N, 11.73%. DSC melting peak: onset 225.0 °C. Selected IR data (cm^{-1}): 1687 (C=O), 1623 (ring C=C), 1603 (ring C=C), 1577 (N=CH), 1500 (NN–H), 1471 (ring C–H bending), 1375 (–OH bending), 1244 (C–OCH_3)

$(HL^2)^+NO_3^-$. Anal. Calcd. for $C_{14}H_{14}N_4O_6$ (334.2843): C, 50.30; H, 4.22; N, 16.76. Found: C, 50.18; H, 3.99; N, 16.57%. DSC: onset 165.0 °C. Selected IR data (cm^{-1}): 1689 (C=O), 1620 (ring C=C), 1608 (ring C=C), 1579 (N=CH), 1500 (NN–H), 1474 (ring C=C), 1460 (–NH), 1375 (–OCH_3), 1326 (N=CH).

$(HL^2)^+HSO_4^-\cdot CH_3OH$.[1] Anal. Calcd. for $C_{14}H_{15}N_3O_7S$ (369.350): C, 45.53; H, 4.09; N, 11.38. Found: C, 45.49; H, 4.20; N, 11.38 %. DSC melting peak: onset 184.0 °C. 1683 (C=O), 1622 (ring C=C), 1607 (ring C=C), 1571 (N=CH), 1504 (NN–H), 1481 (ring C–H bending), 1381 (–OH bending), 1256 (C–OCH_3).

[1] It should be noted that formation of the **$(HL)^+HSO_4^-$** salts were accompanied with a small amount of the 3,3'-dimethoxy-2,2'-dihydroxybenzalazine (CSD code YORROM), or 4,4'-dimethoxy-2,2'-dihydroxybenzalazine (CSD code CIJUV) when the reactions were performed under reflux and upon prolonged reaction time (6 h). Presence of the corresponding azine is proven by the XRD method. The HSO_4^- salts are distinct from the others since the hydrogen sulfate anion is a stronger acid than the protonated hydrazone.

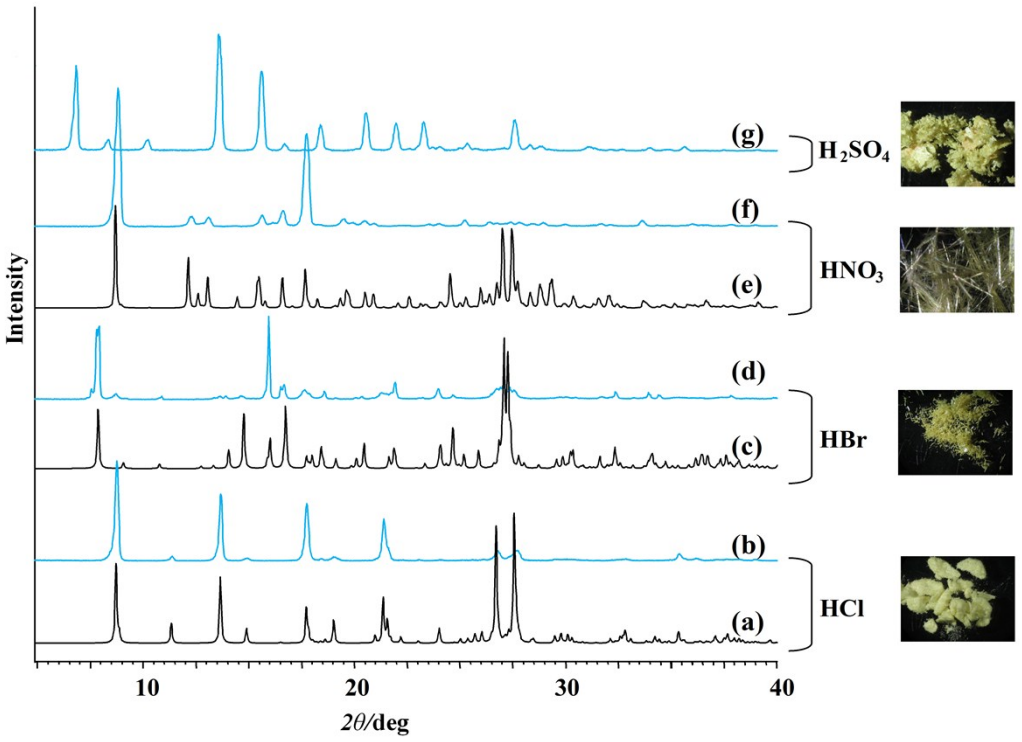

Figure S2. PXRD patterns of **$(HL^2)^+Cl^-\cdot 0.5H_2O$** (a and b); **$(HL^2)^+Br^-\cdot MeOH$** (c and d); **$(HL^2)^+NO_3^-$** (e and f); **$(HL^2)^+HSO_4^-$** (g). The blue lines indicate patterns obtained by powder diffraction, while the black lines indicate patterns calculated from the X-ray single-crystal structures of the corresponding salts.

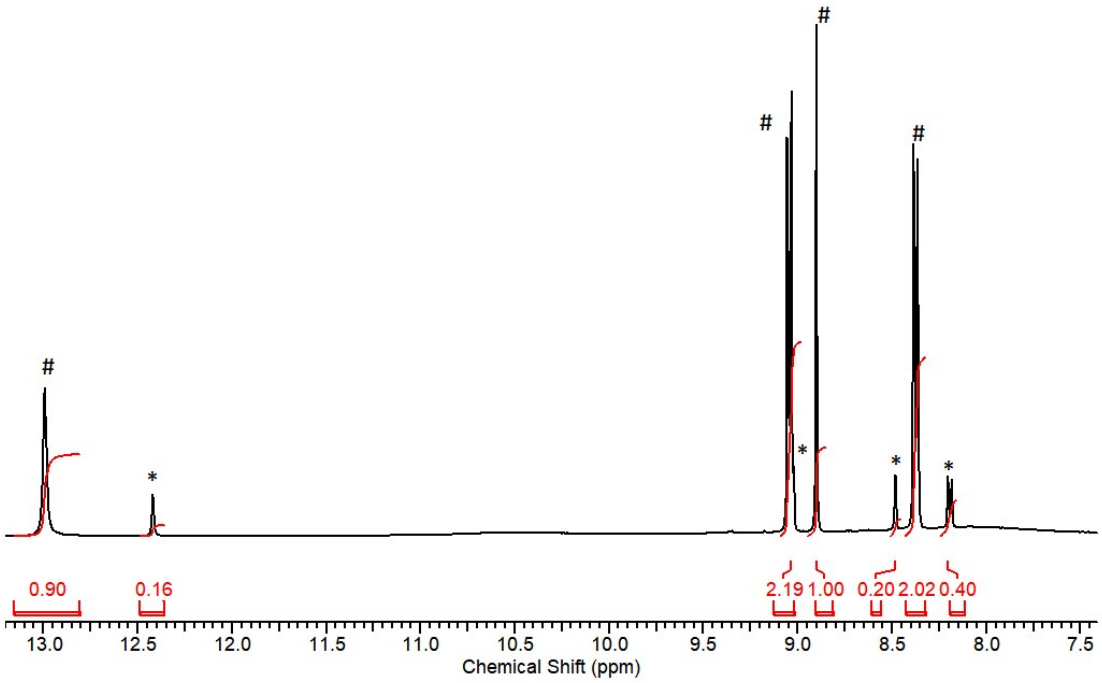

Figure S3. ^{1}H NMR spectra of **$(HL^2)^+Cl^-$** in DMSO-d_6 at room temperature. The signals of *E* isomer and those of Z isomer are marked with # and *, respectively.

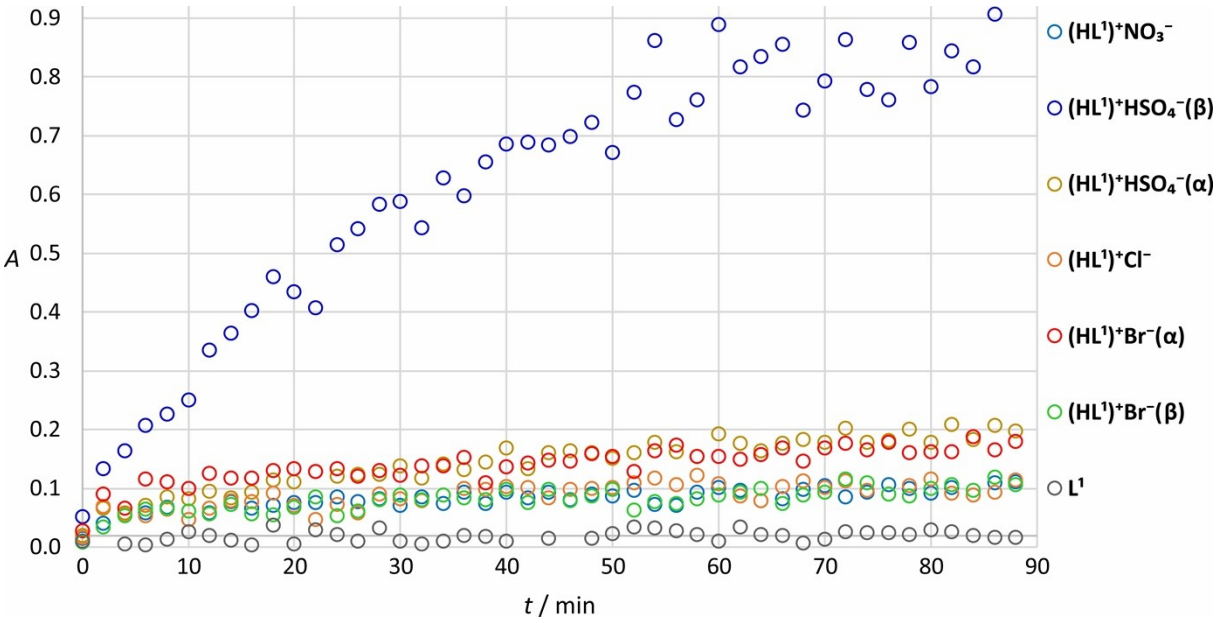

(a)

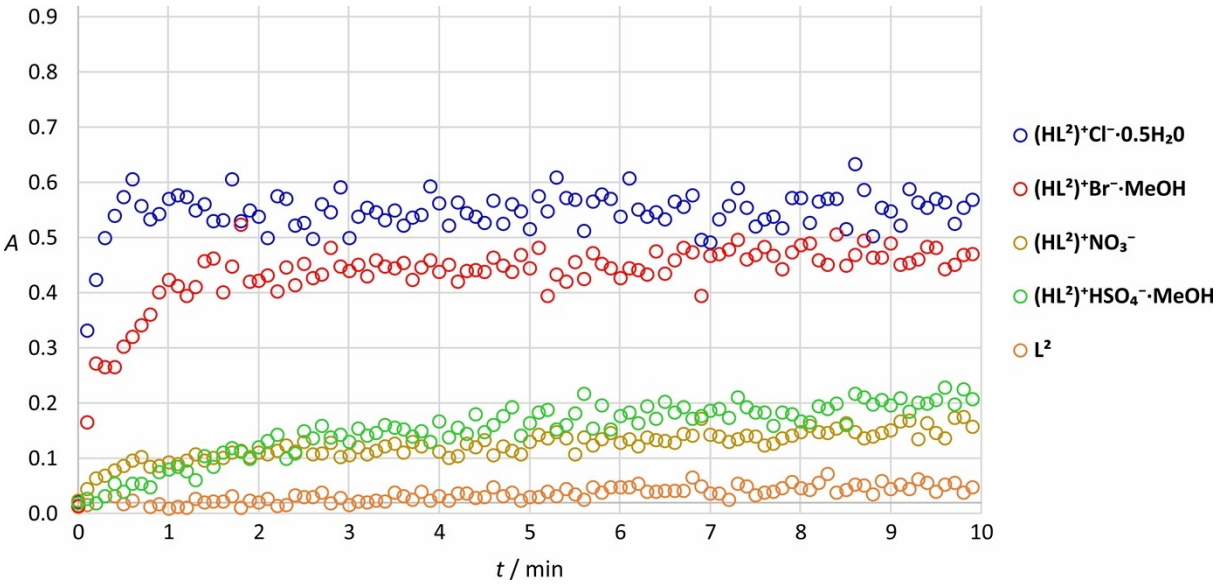

(b)

Figure S4. (a) A comparison of the dissolution profiles between **L¹** and the corresponding salts in water at room temperature; (b) A comparison of the dissolution profiles between **L²** and the corresponding salts in water at room temperature.

3. X-Ray diffraction

Table S1. X-ray powder diffraction crystallographic data for compounds $(HL^1)^+NO_3^-$ and $(HL^1)^+HSO_4^-$ (α and β).

	$(HL^1)^+NO_3^-$	$(HL^1)^+HSO_4^-$ (α)	$(HL^1)^+HSO_4^-$ (β)
chemical formula	$C_{14}H_{14}N_4O_6$	$C_{14}H_{15}N_3O_7S$	$C_{14}H_{15}N_3O_7S$
M_r	334.29	368.35	369.36
powder colour	yellow	orange	yellow
crystal system	triclinic	monoclinic	triclinic
space group	*P*-1	$P\ 2_1/a$	*P*-1
unit cell parameters			
a (Å)	11.4653(3)	7.6971(10)	14.52451(9)
b (Å)	8.3036(2)	33.773(3)	9.07279(5)
c (Å)	8.2387(2)	6.3002(6)	6.81294(3)
α, β, γ (°)	112.057(2), 91.152(2), 91.848(3)	90, 104.838(10), 90	99.7826(4), 93.6851(5), 106.6936(5)
V (Å^3)	726.12(4)	1583.1(3)	841.349(8)
Z	2	4	2
D_{calc} (g cm^{-3})	1.529	1.549	1.450
temperature (K)	293	293	293
wavelength (Å)	1.54060	1.54060	1.54059
R_p	0.0758	0.0512	0.0953
R_{wp}	0.0847	0.0672	0.1363
Starting angle 2Θ (°)	6.5	4.0	2.0
Final angle 2Θ (°)	55	65	135
Step width 2Θ (°)	0.007	0.007	0.013

Table S2. Single-crystal X-ray diffraction crystallographic data for compounds **$(HL^1)^+Cl^-$**, **$(HL^1)^+Br^-$ (α and β)**, **$[H(L^1)_2]^+Br^-$** and **$(HL^1)_2^+SO_4^{2-}$**

	$(HL^1)^+Cl^-$	**$(HL^1)^+Br^-$ (α)**	**$(HL^1)^+Br^-$ (β)**	**$[H(L^1)_2]^+Br^{--}$**	**$(HL^1)_2^+SO_4^{2-}$**
chemical formula	$C_{14}H_{14}ClN_3O_3$	$C_{14}H_{14}BrN_3O_3$	$C_{14}H_{14}BrN_3O_3$	$C_{28}H_{27}BrN_6O_6$	$C_{28}H_{28}N_6O_{10}S$
M_r	307.73	352.18	352.18	623.46	640.62
crystal colour, habit	yellow, plate	orange, plate	yellow, plate	yellow, plate	orange, plate
crystal size (mm^3)	0.52×0.20×0.15	0.48×0.32×0.18	0.50×0.32×0.28	0.56×0.20×0.18	0.52×0.24×0.12
crystal system	triclinic	monoclinic	triclinic	monoclinic	triclinic
space group	*P*-1	$P2_1/c$	*P*-1	*C*2/*c*	*P*-1
unit cell parameters					
a (Å)	7.4513(4)	5.1013(5)	7.4259(3)	17.1019(9)	6.9630(2)
b (Å)	8.2008(4)	36.044(4)	8.4044(3)	13.0795(4)	12.5373(4)
c (Å)	11.4644(6)	8.0122(7)	11.6532(4)	12.6107(5)	16.3477(5)
α, β, γ (°)	92.499(4), 95.861(4), 96.295(4)	90, 92.091(8), 90	92.717(3), 96.841(3), 96.491(3)	90, 98.281(4), 90	84.055(3), 78.144(3), 89.449(3)
V ($Å^3$)	691.62(6)	1472.2(3)	716.11(5)	2791.4(2)	1389.05(8)
Z	2	4	2	4	2
D_{calc} (g cm^{-3})	1.478	1.589	1.633	1.481	1.532
temperature (K)	293	293	293	293	
wavelength (Å)	0.71073	0.71073	0.71073	0.71073	0.71073
μ (mm^{-1})	0.290	2.806	2.884	1.526	0.189
F(000)	320	712	356	1276	668
number of unique	3614	3796	3784	2448	4847
number of data [$F_o \geq 4\sigma(F_o)$]	3098	2321	3450	1988	4498
number of parameters	191	192	190	187	408
R_1[a], [$F_o \geq 4\sigma(F_o)$]	0.0427	0.0578	0.027	0.0376	0.0577
wR_2[b]	0.1285	0.1079	0.0667	0.0867	0.1369
Goodness of fit, *S* [c]	1.04	0.96	1.06	1.04	1.15

min. and max. electron density (e Å^{-3})	-0.30, 0.89	-0.30, 0.64	-0.27, 0.61	-0.23, 0.26	-0.45, 0.49

[a] $R = \Sigma \left| \left| F_o \right| - \left| F_c \right| \right| / \Sigma \left| F_o \right|$; [b] $wR = [\Sigma(F_o^2 - F_c^2)^2 / \Sigma w(F_o^2)^2]^{1/2}$; [c] $S = \Sigma[w(F_o^2 - F_c^2)^2 / (N_{obs} - N_{param})]^{1/2}$

Table S3. Single-crystal X-ray diffraction **c**rystallographic data for compounds **$(HL^2)^+Br^-$·MeOH** and **$(HL^2)^+NO_3^-$**

	$(HL^2)^+Br^-$·MeOH	**$(HL^2)^+NO_3^-$**
chemical formula	$C_{15}H_{18}BrN_3O_4$	$C_{14}H_{14}N_4O_6$
M_r	384.22	334.29
crystal colour, habit	yellow, plate	yellow, needle
crystal size (mm^3)	0.52×0.26×0.14	0.16×0.05×0.01
crystal system	monoclinic	monoclinic
space group	$P2_1/n$	$P2_1/c$
unit cell parameters		
a (Å)	13.3678(9)	21.7477(6)
b (Å)	7.6361(5)	7.4586(2)
c (Å)	16.4545(14)	19.5150(7)
α, β, γ (°)	90, 98.019(7), 90	90, 112.492(4), 90
V ($Å^3$)	1663.2(2)	2924.69(18)
Z	4	8
D_{calc} (g cm^{-3})	1.535	1.518
temperature (K)	150	100
wavelength (Å)	0.71073	0.700
μ (mm^{-1})	2.495	0.116
F(000)	784	1392
number of unique data	2913	8801
number of data [$F_o \geq 4\sigma(F_o)$]	2068	6483
number of parameters	211	437
R_1[a], [$F_o \geq 4\sigma(F_o)$]	0.0546	0.0532
wR_2[b]	0.0796	0.1346
Goodness of fit on F^2, S[c]	1.05	1.02
min. and max. electron density (e $Å^{-3}$)	-0.40, 0.68	-0.31, 0.44

[a] $R = \Sigma \left| \left| F_o \right| - \left| F_c \right| \right| / \Sigma \left| F_o \right|$; [b] $wR = [\Sigma(F_o^2 - F_c^2)^2/\Sigma w(F_o^2)^2]^{1/2}$; [c] $S = \Sigma[w(F_o^2 - F_c^2)^2/(N_{obs} - N_{param})]^{1/2}$

Table S4. Selected bond lengths (Å) and angles (°) for compounds $(HL^1)^+Cl^-$, $(HL^1)^+Br^-$ (α), $(HL^1)^+Br^-$ (β), $[H(L^1)_2]^+Br^-$and $(HL^1)_2^+SO_4^{2-}$.

	$(HL^1)^+Cl^-$	$(HL^1)^+Br^-$ (α)	$(HL^1)^+Br^-$ (β)	$[H(L^1)_2]^+Br^-$	[a] $(HL^1)_2^+SO_4^{2-}$
O1-C2	1.3532(19)	1.364(5)	1.358(2)	1.351(3)	1.352(4), 1.352(5)
O2-C8	1.2132(19)	1.217(5)	1.216(2)	1.216(3)	1.218(4), 1.206(4)
O3-C4	1.3594(19)	1.362(5)	1.358(2)	1.367(3)	1.367(4), 1.356(4)
O3-C14	1.420(2)	1.421(6)	1.427(2)	1.424(4)	1.427(5), 1.437(5)
N1-N2	1.3762(17)	1.383(4)	1.383(2)	1.376(3)	1.374(4), 1.389(4)
N1-C7	1.2815(19)	1.284(5)	1.286(2)	1.278(3)	1.286(5), 1.283(5)
N2-C8	1.3427(19)	1.345(5)	1.343(2)	1.345(3)	1.348(5), 1.351(5)
C1-C7	1.439(2)	1.448(5)	1.443(2)	1.449(3)	1.441(5), 1.448(5)
C8-C9	1.508(2)	1.509(5)	1.507(2)	1.506(3)	1.511(5), 1.516(5)

[a] The labels in the two independent $(HL^1)^+$ ions of $(HL^1)_2^+SO_4^{2-}$ are: O11 and O21, C12 and C22, O12 and O22, C18 and C28, O13 and O23, C14 and C24, O13 and O23, C114 and C214, N11 and N21, N12 and N22, C17 and C27, C18 and C28, C19 and C29

Table S5. Selected bond lengths (Å) and angles (°) for compounds $(HL^2)^+Br^-\cdot MeOH$ and $(HL^2)^+NO_3^-$

	$(HL^2)^+Br^-\cdot$ MeOH	[a] $(HL^2)^+NO_3^-$
O1-C2	1.369(5)	1.359(2), 1.354(2)
O2-C8	1.215(6)	1.217(3), 1.220(2)
O3-C3	1.360(6)	1.363(3), 1.363(2)
O3-C14	1.443(5)	1.433(2), 1.432(3)
N1-N2	1.374(5)	1.382(2), 1.378(2)
N1-C7	1.285(6)	1.285(3), 1.285(3)
N2-C8	1.362(5)	1.368(3), 1.364(3)
C1-C7	1.463(6)	1.458(3), 1.460(3)
C8-C9	1.517(6)	1.511(3), 1.514(3)

[a] The labels in the two independent $(HL^2)^+$ ions of $(HL^2)^+NO_3^-$ are: O11 and O21, C12 and C22, O12 and O22, C18 and C28, O13 and O23, C13 and C23, O13 and O23, C114 and C214, N11 and N21, N12 and N22, C17 and C27, C18 and C28, C19 and C29.

Table S6. Geometry of intra- and intermolecular hydrogen bonds (Å, °) for compounds **$(HL^1)^+Cl^-$**, **$(HL^1)^+Br^-$** (α and β), **$[H(L^1)_2]^+Br^-$**, **$(HL^1)_2^+SO_4^{2-}$**, **$(HL^2)^+Br^-$·MeOH** and **$(HL^2)^+NO_3^-$**

	D-H···A	D-H (Å)	H···A (Å)	D···A (Å)	D-H···A(°)
$(HL^1)^+Cl^-$	O1-H1···N1	0.82	1.86	2.5872(17)	147
	N2-H2···Cl^{i}	0.86	2.40	3.1475(13)	146
	N3-H3···Cl^{ii}	0.86	2.16	3.0100(14)	170
$(HL^1)^+Br^-$ (α)	O1-H1···N1	0.82	1.89	2.610(4)	146
	N2-H2···Br	0.86	2.77	3.407(3)	132
	N3-H3···Br	0.86	2.48	3.243(3)	148
$(HL^1)^+Br^-$ (β)	O1-H1···N1	0.82	1.88	2.605(2)	147
	N2-H2···Br	0.86	2.54	3.3062(14)	149
	N3-H3···Br^{iii}	0.86	2.32	3.1706(16)	170
$[H(L^1)_2]^+Br^-$	O1-H1···N1	0.82	1.85	2.569(3)	146
	N2-H2···Br	0.86	2.67	3.388(2)	142
	N3-H3···N3^{iv}	0.86	1.84	2.688(3)	168
$(HL^1)_2^+SO_4^{2-}$	O11-H11···N11	0.82	1.87	2.591(4)	146
	N12-H12N···O1S^{v}	0.86	2.24	2.931(4)	137
	N13-H13N···O3S	0.86	1.83	2.676(3)	169
	O21-H21O···N21	0.82	1.86	2.587(4)	147
	N22-H22N···O2S	0.86	2.18	2.769(4)	126
	N23-H23N···O3S	0.86	1.83	2.684(3)	173
$(HL^2)^+Br^-$·MeOH	O1-H1 N1^{vi}	0.82	1.90	2.616(5)	146
	N2-H2 Br1^{vii}	0.86	2.66	3.482(3)	159
	N3-H3 Br1	0.86	2.37	3.209(4)	167
	O4-H4O Br1	0.82	2.53	3.325(3)	164
$(HL^2)^+NO_3^-$	O11-H11 N11	0.82	1.91	2.6632(2)	145
	N12-H12 O15^{viii}	0.86	2.20	3.031(2)	162
	N13-H13 O14	0.86	1.88	2.710(2)	163
	N13-H13 O15	0.86	2.52	3.181(2)	135
	O21-H21 N21	0.82	1.89	2.6076(18)	145
	N22-H22 O25^{viii}	0.86	2.08	2.9169(19)	164
	N23-H23 O24^{ix}	0.86	1.92	2.771(2)	171
	N23-H23 O25^{ix}	0.86	2.47	3.0983(19)	130

^{i}1-x,2-y,1-z; ^{ii}x,1+y,z; ^{iii}2-x,2-y,1-z; ^{iv}1-x,y,-1/2-z; ^{v}-x,3-y,2-z; ^{vi}x,-1+y,z; ^{vii}3/2-x,-1/2+y,3/2-z; ^{viii}x,1/2-y,1/2+z; ^{ix}x,1/2-y,1/2+z

Table S7. Geometric parameters of the aromatic stacking interactions for compounds **$(HL^1)^+Cl^-$**, **$(HL^1)^+Br^-$** (β) , **$[H(L^1)_2]^+Br^-$** , **$(HL^1)_2^+SO_4^{2-}$, $(HL^2)^+Br^-$·MeOH** and **$(HL^2)^+NO_3^-$**

	Cg···*Cg* /Å	slippage /Å
$(HL^1)^+Cl^-$	*d*(*C*g1···*C*g2)^{i} =3.6321(9)	1.28
$(HL^1)^+Br^-$ (β)	*d*(*C*g1···*C*g2)^{ii}= 3.6640(10)	1.37
$[H(L^1)_2]^+Br^-$	*d*(*C*g1···*C*g2)^{iii}=4.0010(15)	2.09
$(HL^1)_2^+SO_4^{2-}$	*d*(*C*g1···*C*g1)^{iv}=3.6592(18)	1.67
	d(*C*g3···*C*g3)^{v}=3.9114(18)	2.24
$(HL^2)^+Br^-$·MeOH	*d*(*C*g1···*C*g2)^{ii}=3.532(2)	1.19
$(HL^2)^+NO_3^-$	*d*(*C*g1···*C*g2)^{ii}=3.5663(9)	1.21
	d(*C*g3···*C*g4)v^{ii}=3.4954(9)	1.21

^{i} −*x*,3−*y*,1−*z*; ^{ii} 1−x,1−y,1−z; ^{iii}1−*x*, *y*, 1/2−*z*; ^{iv} −*x*,3−*y*,2−*z*; ^{v}-2−*x*, 2−*y*, 2−*z*; ^{vi}−*x*, −*y*,1−*z*

*C*g1 is the centroid of the pyridine ring N3, C9−C13, *C*g2 is the centroid of the phenyl ring C−C6 and *C*g4 is the centroid of the ring C8−C13

In **$(HL^1)_2^+SO_4^{2-}$** Cg1 and Cg3 are centroids of the pyridine rings N13, C19–C113 and N23, C29–C213, respectively

In **$(HL^2)^+NO_3^-$** Cg1 and Cg3 are centroids of the pyridine rings N13, C19–C113 and N23, C29–C213 and Cg1 and Cg3 are centroids of the pheyl rings C11–C16 and C21–C26

Table S8. Structural motifs in investigated compounds. The first row shows type of the hydrogen bond interaction and symbol for each interaction. All other interactions are of the van der Waals type.

Type of interaction	D–H···A D = N,O; A = acceptor from anion				C–H···A A = acceptor from ion					
Symbol										
Comp.	**$(HL^1)^+Cl^-$**	**$(HL^1)^+Br^-$ (α)**	**$(HL^1)^+Br^-$ (β)**	**$[H(L^1)_2]^+Br^-$**	**$(HL^1)^+NO_3^-$**	**$(HL^1)^+HSO_4^-$ (α)**	**$(HL^1)^+HSO_4^-$ (β)**	**$(HL^1)_2^+SO_4^{2-}$**	**$(HL^2)^+Br^-$ ·MeOH**	**$(HL^2)^+NO_3^-$**
0D	dimer	dimer 	dimer							
1D				chain 	ribbon 		ribbon 	double chain	chain 	chain 
2D	double layer		double layer	layer 	layer 	layer 	layer 			
3D										

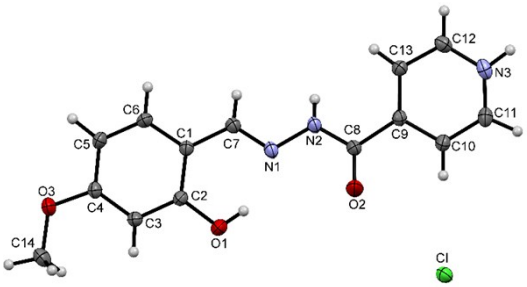

$(HL^1)^+Cl^-$

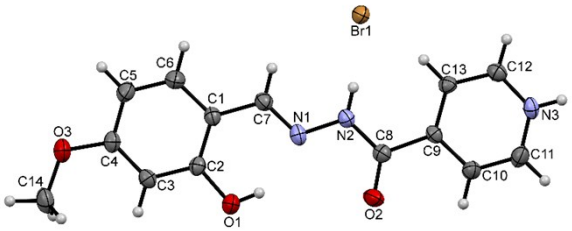

$(HL^1)^+Br^-$ (α)

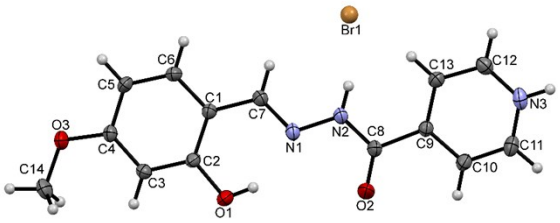

$(HL^1)^+Br^-$ (β)

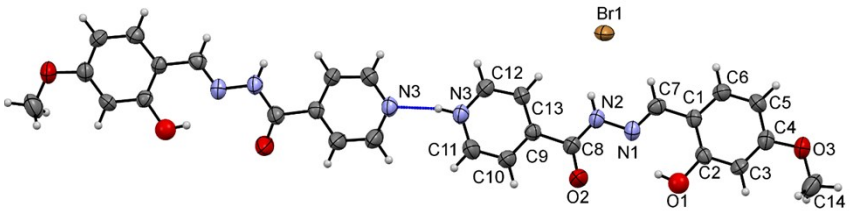

$[H(L^1)_2]^+Br^-$

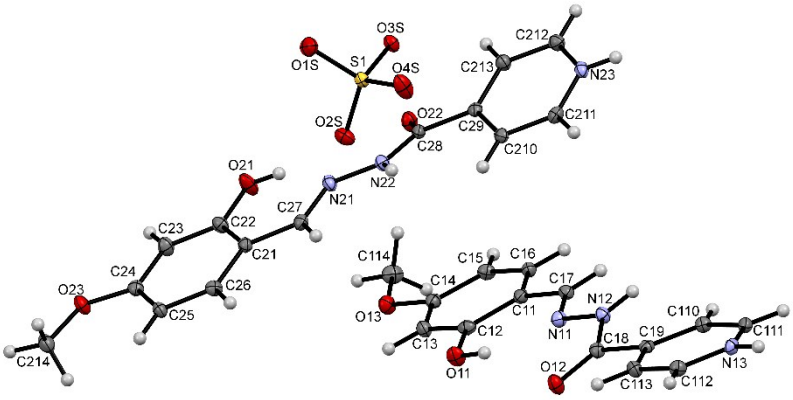

$(HL^1)_2^+SO_4^{2-}$

Figure S5. ORTEP drawing of asymmetric unit of **$(HL^1)^+Cl^-$, $(HL^1)^+Br^-$** (α and β), **$[H(L^1)_2]^+Br^-$** and **$(HL^1)_2^+SO_4^{2-}$**. Displacement ellipsoids of non-hydrogen atoms are drawn at 50 % probability level.

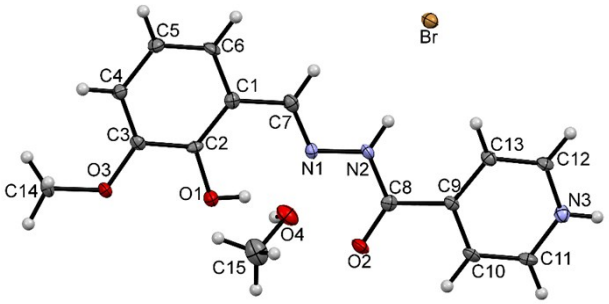

$(HL^2)^+Br^-\cdot MeOH$

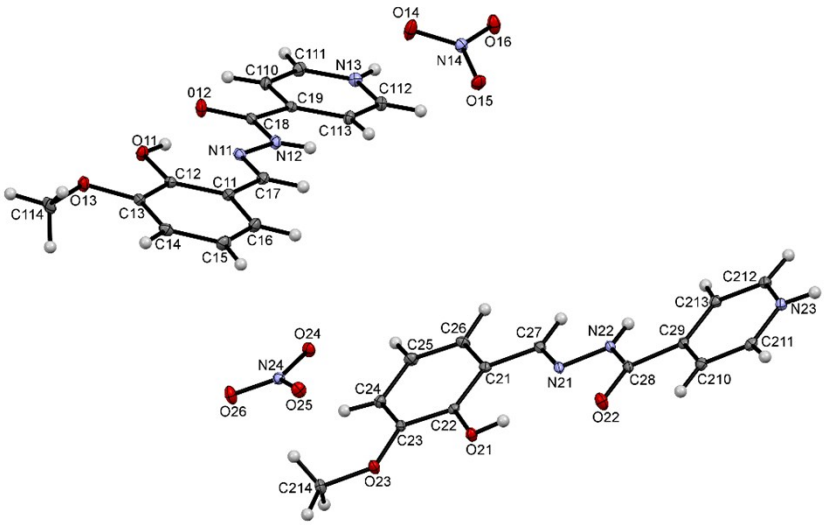

$(HL^2)^+NO_3^-$

Figure S6. ORTEP drawing of asymmetric unit of **$(HL^2)^+Br^-\cdot MeOH$** and **$(HL^2)^+NO_3^-$**. Displacement ellipsoids of non-hydrogen atoms are drawn at 50 % probability level.

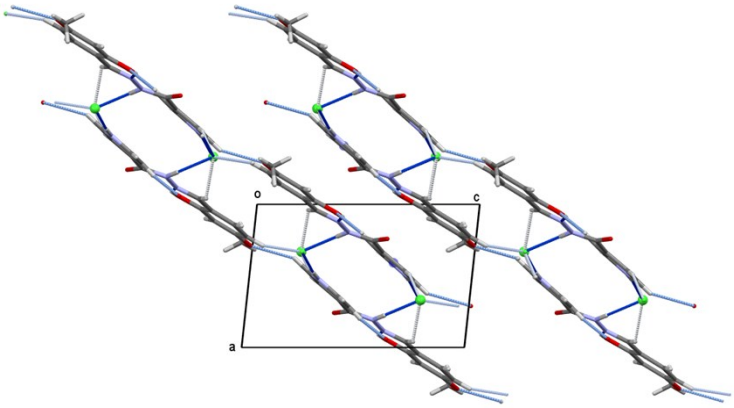

Figure S7. Hydrogen bonds in two selected 2D layers in **$(HL^1)^+Cl^-$**. Hydrogen bonds are shown as dashed blue lines.

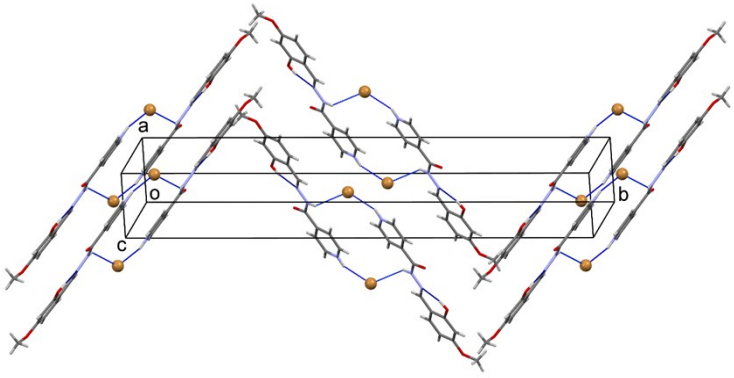

Figure S8. Packing diagram of **$(HL^1)^+Br^-$** (α) showing herringbone structural motif**.** N–H···Br and O–H···N type hydrogen bonds are shown by blue dotted lines while weak type C–H···Br and C–H···O hydrogen bonds are omitted for clarity.

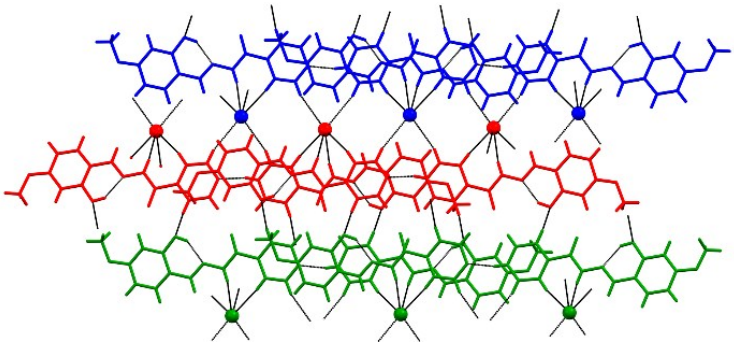

Figure S9. Infinite 2D layer in **$[H(L^1)_2]^+Br^-$** formed by weak C–H···Br and C–H···O (O is oxygen atom from hydroxide group) interactions between three neighboring chains (chains are presented by different colors).

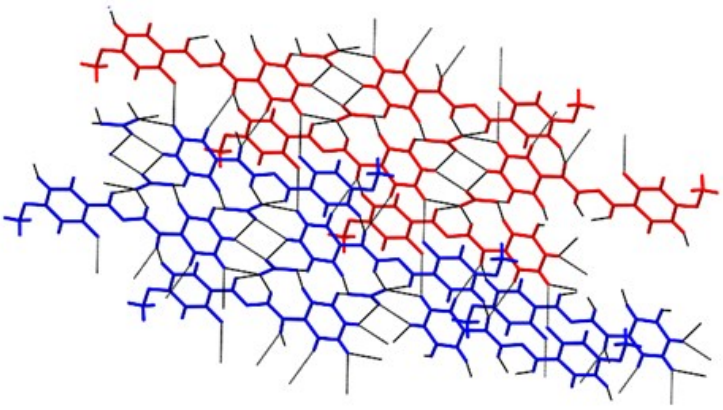

Figure S10. Weak C–H···O interactions (O is hydrogen atom from hydroxyl and carbonyl group) connecting ribbons in **$(HL^1)^+NO_3^-$**. Two ribbons are presented with different colours (red and blue colours). Hydrogen bonds are shown by black dotted lines.

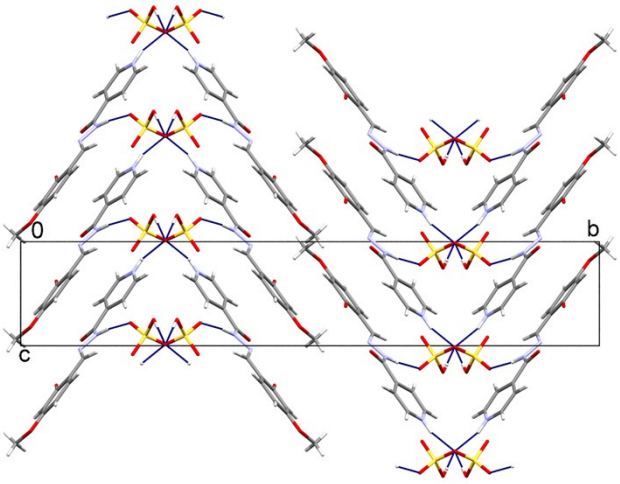

Figure S11. Packing diagram of **$(HL^1)^+HSO_4^-$** (α) showing herringbone structural motif**.** N2–H2···O4[1/2+x,3/2-y,-1+z], N3–H3···O7 and O5–H2···O7 hydrogen bonds are shown by blue dotted lines.

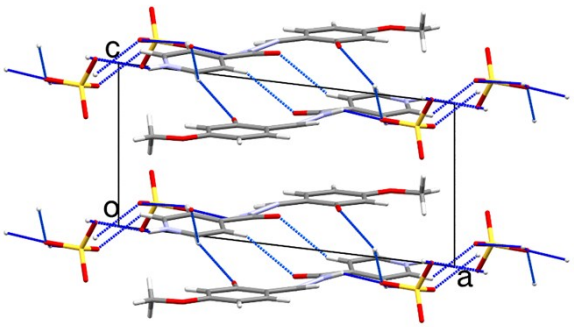

Figure S12. Packing diagram of **$(HL^1)^+HSO_4^-$** (β). Four ribbons are presented. Hydrogen bonds are shown by blue dotted lines.

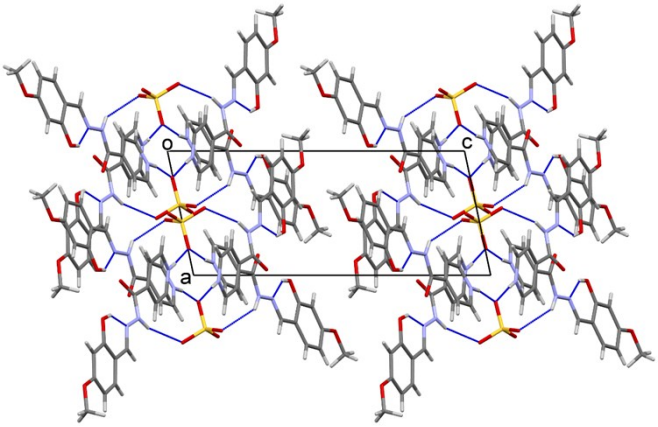

Figure S13. Packing diagram of $(HL^1)_2^+SO_4^{2-}$. Hydrogen bonds are shown by blue dotted lines.

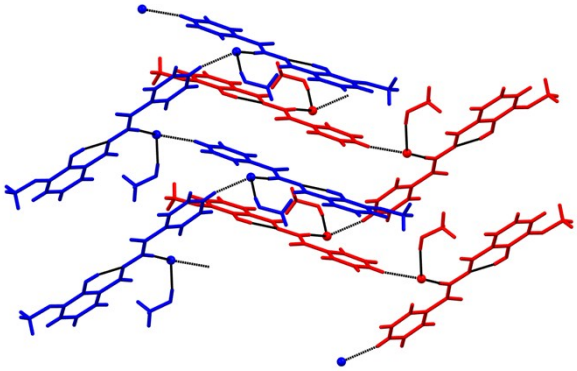

Figure S14. Interaction between two chains (red and blue colour) in $(HL^2)^+Br^-\cdot MeOH$. Hydrogen bonds within the chain are shown as dashed black lines.

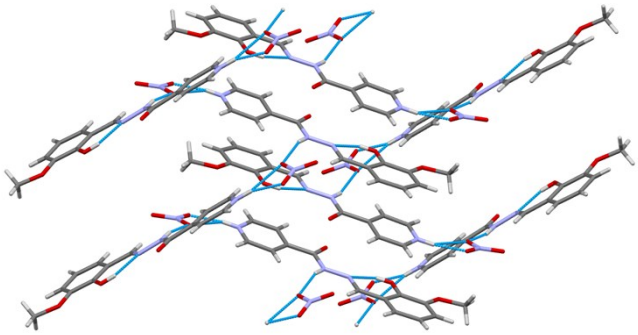

Figure S15. Interaction between two infinite 1D zig-zag chain of one independent pair of cation and anion in $(HL^2)^+NO_3^-$. Hydrogen bonds N13–H3···O14, N13–H3···O15 and N12–H2···O15 [1-x,1/2+y,3/2-z] within the chain are shown as dashed blue lines.

4. *UV-Vis spectroscopy*

Spectral data

L[1]: UV-Vis (CH_3CN) λ/nm: 219 (ε = 21999 cm^{-1} mol^{-1} dm^3). 249 (ε = 12768 cm^{-1} mol^{-1} dm^3). 294 (ε = 12034 cm^{-1} mol^{-1} dm^3). 308 (ε = 14931 cm^{-1} mol^{-1} dm^3) and 334 (ε = 23494 cm^{-1} mol^{-1} dm^3).

$(HL^1)^+Cl^-$: UV-Vis (CH_3CN) λ/nm: 221 (ε = 5486 cm^{-1} mol^{-1} dm^3). 244 (ε = 3089 cm^{-1} mol^{-1} dm^3). 295 (ε = 3660 cm^{-1} mol^{-1} dm^3). 305 (ε = 3444 cm^{-1} mol^{-1} dm^3) and 338 (ε = 4461 cm^{-1} mol^{-1} dm^3).

$(HL^1)^+Br^-$: UV-Vis (CH_3CN) λ/nm: 223 (ε = 28535 cm^{-1} mol^{-1} dm^3). 245 (ε = 11106 cm^{-1} mol^{-1} dm^3). 291 (ε = 13899 cm^{-1} mol^{-1} dm^3). 306 (ε = 10587 cm^{-1} mol^{-1} dm^3) and 354 (ε = 11590 cm^{-1} mol^{-1} dm^3).

$(HL^1)^+NO_3^-$: UV-Vis (CH_3CN) λ/nm: 219 (ε = 25235 cm^{-1} mol^{-1} dm^3). 244 (ε = 12283 cm^{-1} mol^{-1} dm^3). 295 (ε = 13637 cm^{-1} mol^{-1} dm^3). 305 (ε = 13160 cm^{-1} mol^{-1} dm^3) and 337 (ε = 17267 cm^{-1} mol^{-1} dm^3).

$(HL^1)^+HSO_4^-$: UV-Vis (CH_3CN) λ/nm: 223 (ε = 9873 cm^{-1} mol^{-1} dm^3). 245 (ε = 5554 cm^{-1} mol^{-1} dm^3). 292 (ε = 6959 cm^{-1} mol^{-1} dm^3). 306 (ε = 5512 cm^{-1} mol^{-1} dm^3) and 349 (ε = 6044 cm^{-1} mol^{-1} dm^3).

L[2]: UV-Vis (CH_3CN) λ/nm: 223 (ε = 20632 cm^{-1} mol^{-1} dm^3), 278 (ε = 12296 cm^{-1} mol^{-1} dm^3) and 304 (ε = 10081 cm^{-1} mol^{-1} dm^3).

$(HL^2)^+Cl^-$: UV-Vis (CH_3CN) λ/nm: 225 (ε = 25747 cm^{-1} mol^{-1} dm^3). 278 (ε = 14481 cm^{-1} mol^{-1} dm^3). and 305 (ε = 15598 cm^{-1} mol^{-1} dm^3).

$(HL^2)^+Br^-$: UV-Vis (CH_3CN) λ/nm: 223 (ε = 28690 cm^{-1} mol^{-1} dm^3). 277 (ε = 12995 cm^{-1} mol^{-1} dm^3) and 305 (ε = 10786 cm^{-1} mol^{-1} dm^3).

$(HL^2)^+NO_3^-$: UV-Vis (CH_3CN) λ/nm: 223 (ε = 19543 cm^{-1} mol^{-1} dm^3). 277 (ε = 9576 cm^{-1} mol^{-1} dm^3) and 304 (ε = 12093 cm^{-1} mol^{-1} dm^3).

$(HL^2)^+HSO_4^-$: UV-Vis (CH_3CN) λ/nm: 226 (ε = 20679 cm^{-1} mol^{-1} dm^3). 276 (ε = 12342 cm^{-1} mol^{-1} dm^3) and 304 (ε = 10109 cm^{-1} mol^{-1} dm^3).

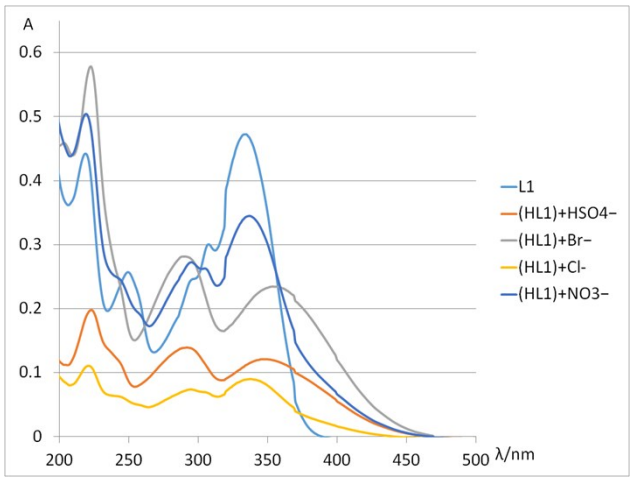

(a)

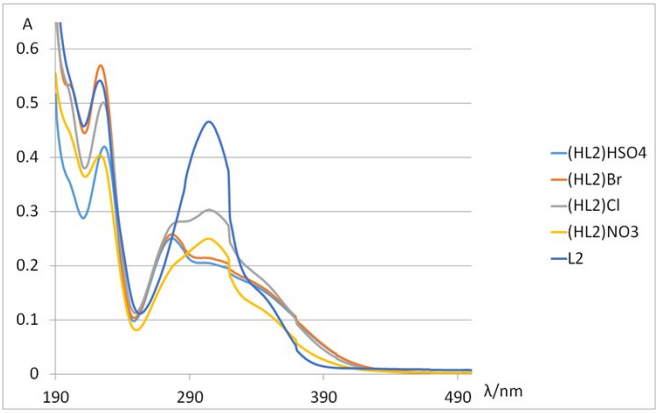

(b)

Figure S16. The UV/Vis spectra of a) **L**[1] and salts and b) **L**[2] and salts in acetonitrile.

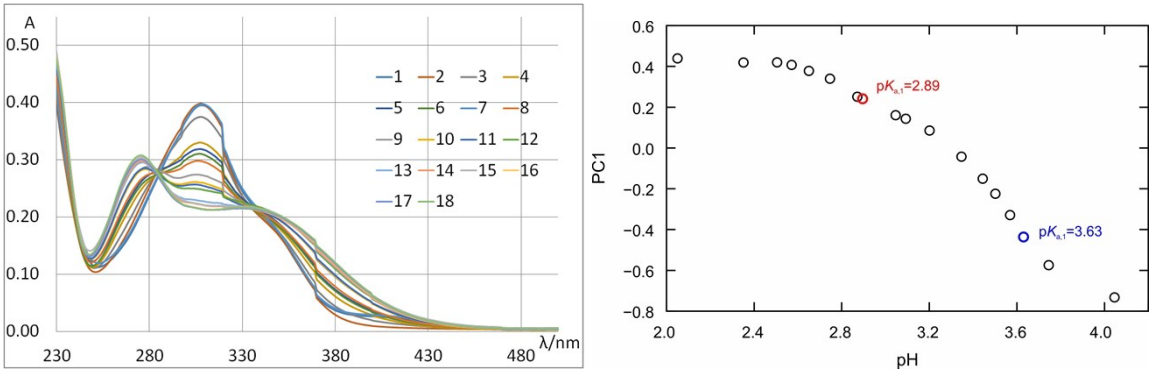

Figure S17. The UV/Vis spectra of **L²** upon titration with HCl in methanol; b) PC1 scores calculated by principal component analysis performed for a set of UV/Vis spectra of **L²** titrated with HCl in methanol (pK_a values were determined by nonlinear regression on generalised logistic curve).

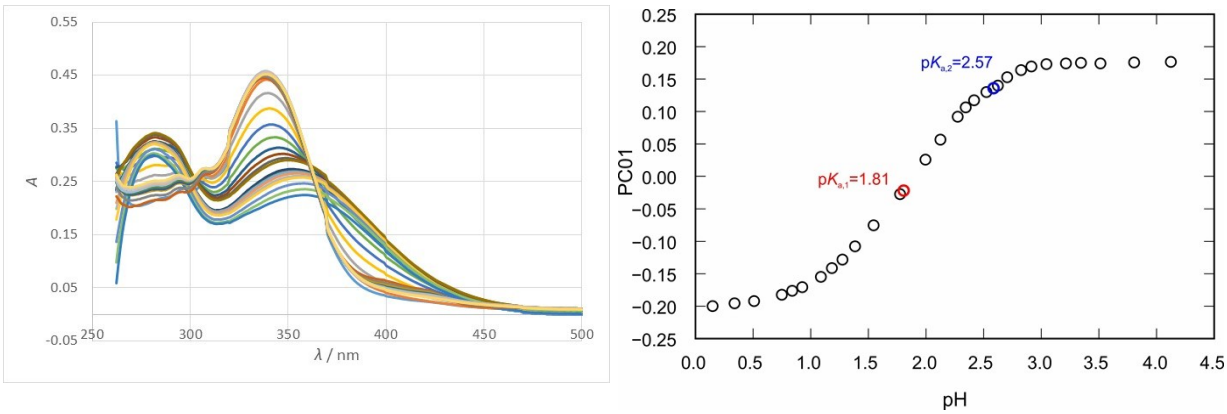

Figure S18. The UV/Vis spectra of **L¹** upon titration with H_2SO_4 in DMSO; b) PC01 scores calculated by principal component analysis performed for a set of UV/Vis spectra of **L¹** titrated with H_2SO_4 in DMSO (pK_a values were determined by nonlinear regression on generalised logistic curve).

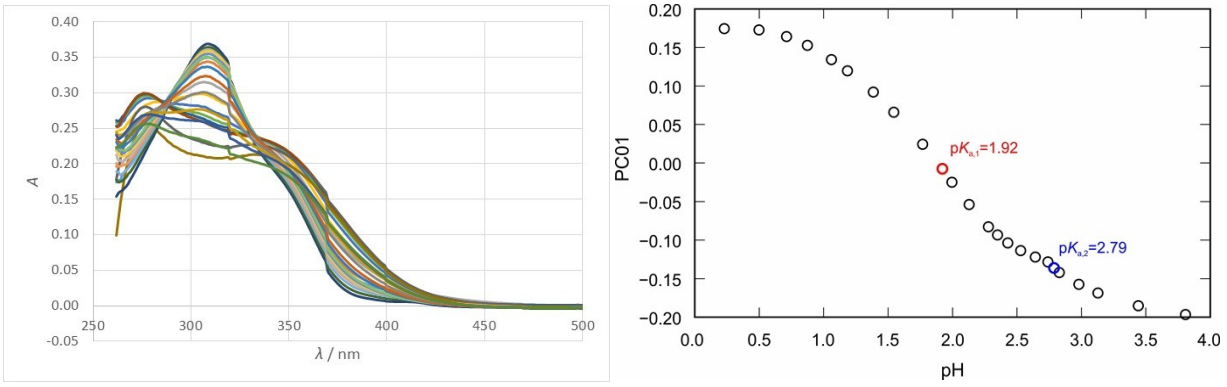

Figure S19. The UV/Vis spectra of **L²** upon titration with H_2SO_4 in DMSO; b) PC01 scores calculated by principal component analysis performed for a set of UV/Vis spectra of **L²** titrated with H_2SO_4 in DMSO (pK_a values were determined by nonlinear regression on generalised logistic curve).

Multivariate Data Analysis*:** numerical analyses were performed using the second order tensor analysis tool principal component analysis PCA where data matrix (or two-way array) ***X of rank *r* is decomposed as a sum of *r* matrices of rank 1

$$\sum$$

where stands for score and for loading vectors. PCA finds the best linear projections for a high dimensional set of data in the least squares sense. Scores represent projections of the original points on the principal component (PC) direction and can be used for classification. whereas loadings represent eigenvectors of data covariance (or correlation) matrix and can be used for the identification of variability among the data.

5. *NMR spectroscopy*

Experimental details. All the NMR spectra were recorded on a Bruker Avance 300 NMR spectrometer operating at 300 MHz for ^{1}H and 75 MHz for ^{13}C using a C/H dual 5 mm probe. The spectra were recorded in DMSO-d_6 with a sample concentration of 20 mg ml^{-1} and TMS as the internal standard. ^{1}H NMR spectra with spectral width of 6200 Hz and a digital resolution of 0.09 Hz per point were measured with 32 scans. APT spectra with spectral widths of 17985 Hz were collected with 10240 scans. Digital resolution was 0,27 Hz per point. In the gCOSY experiment 2048 points in the *f*2 dimension and 256 increments in the *f*1 dimension were used. For each increment 16 scans and the spectral width of 4006 Hz were applied. Digital resolution was 1,95 and 15,65 Hz per point in *f*2 and *f*1 dimensions, respectively. Spectral width of gHMQC spectra was 3086 and 11647 Hz in *f*2 and *f*1 dimensions, respectively. 1K data points were used in the time domain and 256 increments were collected for each data set. The resulting digital resolution was 3.01 and 45.49 Hz per point in *f*2 and *f*1 dimensions, respectively. Spectral width for gHMBC spectra was 3906 and 16762 Hz in *f*2 and *f*1 dimensions, respectively. In the time domain, 4K data points were applied. The number of increments for each data set was 256. The acquired spectra had digital resolution of 0.95 and 65.48 Hz per point in *f*2 and *f*1 dimensions, respectively.

Scheme S2. The structural formula of **L¹** and **L²** with the NMR numbering scheme (with 4-methoxy and 3-methoxy substituent as R, respectively)

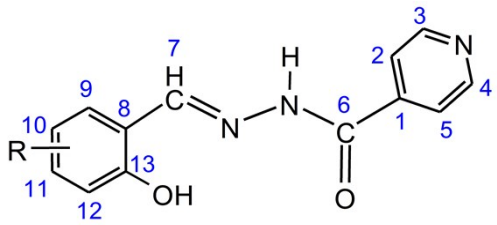

Table S9. ^{1}H and ^{13}C chemical shifts for **L^1**, **$(HL^1)^+ Cl^-$**, **$(HL^1)^+ Br^-$**, **$[H(L^1)_2]^+Br^-$**, **$(HL^1)^+NO_3^-$**, **$(HL^1)^+ HSO_4^-$** and **$(HL^1)_2^{2+}SO_4^{2-}$**

Compound	**L^1**		**$(HL^1)^+ Cl^-$**		**$(HL^1)^+ Br^-$ (α)**		**$[H(L^1)_2]^+Br^-$**	
Atom	δ / ppm (^{1}H)	δ / ppm (^{13}C)	δ / ppm (^{1}H)	δ/ ppm (^{13}C)	δ / ppm (^{1}H)	δ / ppm (^{13}C)	δ / ppm (^{1}H)	δ / ppm (^{13}C)
1	-	140.53	-	146.06	-	146.19	-	144.34
2,5	7.845	122.18	8.392	124.78	8.326	124.71	8.161	123.77
3,4	8.823	151.03	9.044	150.76	9.081	150.51	8.997	150.33
6	-	161.63	-	160.15	-	159.91	-	160.29
7	8.606	150.12	8.788	145.17	8.689	145.65	8.667	147.25
8	-	112.27	-	112.09	-	112.14	-	112.11
9	6.559	131.50	6.541	131.18	6.552	131.23	6.555	131.27
10	7.497	107.10	7.496	107.10	7.523	107.22	7.518	107.08
11	-	163.01	-	162.95	-	163.05	-	163.00
12	6.519	101.47	6.522	101.61	6.514	101.63	6.500	101.59
13	-	159.90	-	159.65	-	159.75	-	159.96
NH	12.228	-	12,964	-	12,582	-	12,449	-
OH	11.460	-		-		-		-
CH_3O	3.774	55,81	3,780	55,94	3,780	55,84	3.770	56,13

Compound	**$(HL^1)^+NO_3^-$**		**$(HL^1)^+HSO_4^-$ (α)**		**$(HL^1)_2^{2+}SO_4^{2-}$**	
Atom	δ / ppm (^{1}H)	δ / ppm (^{13}C)	δ / ppm (^{1}H)	δ / ppm (^{13}C)	δ / ppm (^{1}H)	δ / ppm (^{13}C)
1	-	146.02	-	146.19	-	147.78
2,5	8.265	124.50	8.31	122.29	8.114	123.71
3,4	9.050	150.52	9.071	150.86	8.945	150.36
6	-	159.90	-	159.947	-	160.59
7	8.623	145.89	8.672	145.70	8.648	143.79
8	-	112.15	-	112.14	-	112.14
9	6.554	131.21	6.566	131.45	6.565	131.29
10	7.528	107.21	7.526	107.12	7.479	107.21
11	-	163.04	-	163.14	-	163.08
12	6.497	101.56	6.516	101.04	6.395	101.61
13	-	159.82	-	157.70	-	159.76
NH	12,473	-	12.475	-	12.387	-
OH	11,337	-		-		-
CH_3O	3.781	55.56	3.810	55.90	3.824	55.00

Table S10. ^{1}H and ^{13}C chemical shifts for **L^2**, **$(HL^2)^+Cl^-$**, **$(HL^2)^+Br^-$**, **$(HL^2)^+NO_3^-$** and **$(HL^2)^+HSO_4^-$**

Compound	**L^2**		**$(HL^2)^+Cl^-$**		**$(HL^2)^+Br^-$**		**$(HL^2)^+NO_3^-$**		**$(HL^2)^+HSO_4^-$**	
Atom	δ / ppm (^{1}H)	δ / ppm (^{13}C)	δ / ppm (^{1}H)	δ/ ppm (^{13}C)	δ / ppm (^{1}H)	δ / ppm (^{13}C)	δ / ppm (^{1}H)	δ / ppm (^{13}C)	δ / ppm (^{1}H)	δ / ppm (^{13}C)
1	-	140.43	-	145.52	-	145.97	-	146.03	-	146.09
2,5	7.854	120.95	8.266	120.81	8.302	120.69	8.266	120.69	8.310	120.49
3,4	8.794	151.03	9.056	150.41	9.094	149.84	9.056	150.16	9.072	149.97
6	-	161.94	-	160.07	-	160.07	-	160.32	-	160.07
7	8.700	149.41	8.749	145.96	8.811	145.71	8.749	145.63	8.771	145.71
8	-	119.16	-	119.29	-	119.29	-	119.35	-	119.29
9	7.212	122.02	7.820	124.61	7.221	124.50	7.280	124.62	7.219	124.69
10	6.878	119.44	6.880	119.60	6.859	119.80	6.880	119.60	6.891	119.80
11	7.055	114.14	7.082	114.59	7.071	114.71	7.082	114.63	7.066	114.52
12	-	148.50	-	148.51	-	148.51	-	148.31	-	148.52
13	-	147.36	-	147.62	-	147.74	-	147.74	-	147.62
NH	12.283	-	13.003	-	12.586	-	12.498	-	12.564	-
OH	10.716	-	12.411	-		-	10.613	-		-
CH_3O	3.833	55.46	3.804	56.34	3.818	56.15	3.804	55.34	3.821	56.34

Table S11. ^{13}C CP-MAS chemical shifts for **L^1**, **$(HL^1)^+Cl^-$**, **$(HL^1)^+$ Br^-(α** and **β)**, **$[H(L^1)_2]^+Br^-$**, **$(HL^1)^+NO_3^-$**, **$(HL^1)^+$ HSO_4^-(α)**, **$(HL^1)_2^{2+}SO_4^{2-}$** and **$(HL^1)^+HSO_4^-$(β).**

	L^1	**$(HL^1)^+Cl^-$**	**$(HL^1)^+Br^-$ (α)**	**$(HL^1)^+$ Br^- (β)**	**$[H(L^1)_2]^+Br^-$**	**$(HL^1)^+NO_3^-$**	**$(HL^1)^+HSO_4^-$ (α)**	**$(HL^1)_2^{2+}SO_4^{2-}$**	**$(HL^1)^+HSO_4^-$ (β)**
Atom	δ / ppm (^{13}C)	δ / ppm (^{13}C)	δ / ppm (^{13}C)	δ / ppm (^{13}C)	δ / ppm (^{13}C)	δ / ppm (^{13}C)	δ / ppm (^{13}C)	δ / ppm (^{13}C)	δ / ppm (^{13}C)
1	133.68	132.63	134.91	134.02	132.74	133.13	133.09	136.44	135.42
2.5	122.56	125.26	124.75	124.13	125.14	125.00	124.66	125.77	125.51
3.4	149.60	148.62	146.35	148.35	148.97	148.38	145.91	148.61	148.89
6	161.54	159.01	162.61	161.88	157.09	160.23	161.60	161.59	156.76
7	142.74	142.76	143.04	143.45	141.51	144.82	140.09	143.81	144.57
8	111.45	112.56	112.30	112.40	112.42	113.63	112.15	112.05	112.30
9	125.31	128.56	131.61	125.17	128.63	127.59	131.06	128.62	128.05
10	110.07	109.00	109.74	109.63	108.47	110.78	110.81	106.12	110.52
11	161.74	164.39	165.40	164.29	163.74	163.66	166.06	163.40	161.59
12	99.92	103.66	101.88	100.61	104.24	100.11	101.43	104.17	99.95
13	151.03	154.73	154.48	152.49	155.25	159.03	156.38	156.76	156.76
CH_3O	55.45	57.67	55.13	56.09	57.31	57.67	56.60	55.64	56.56

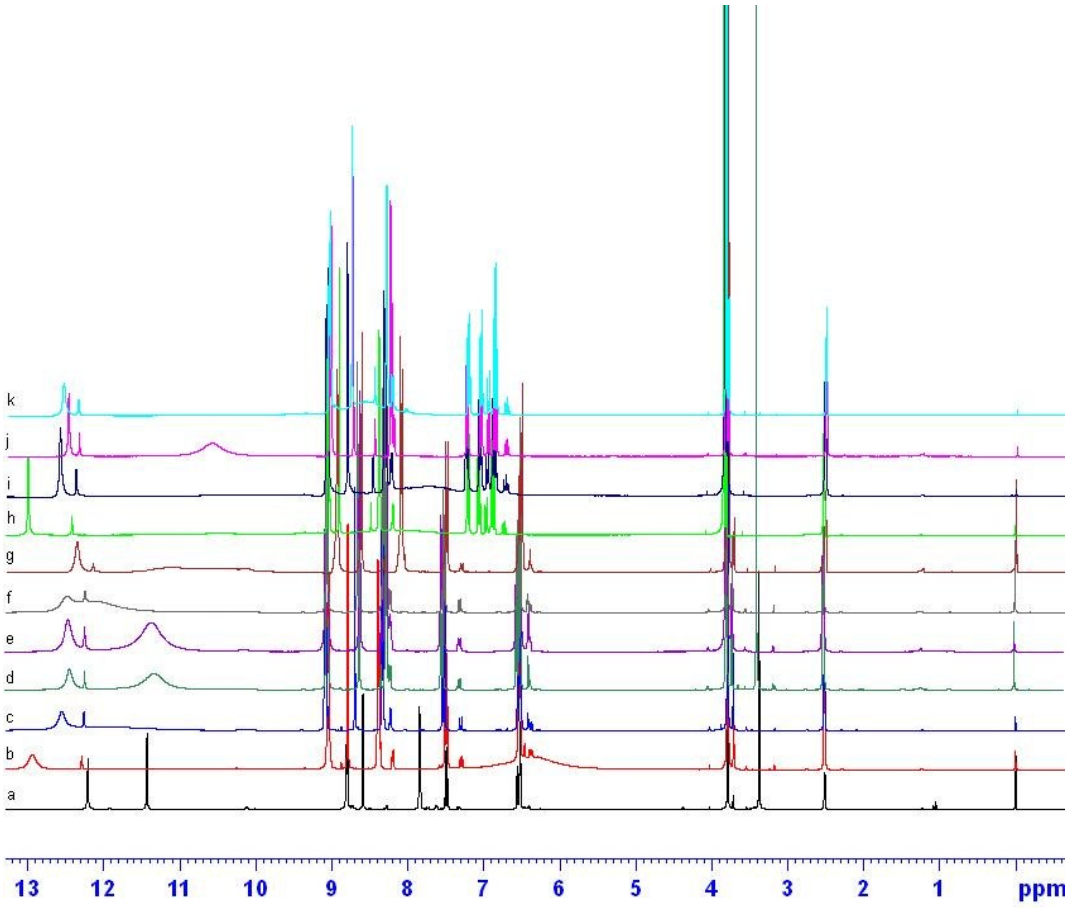

Figure S20. ^{1}H NMR spectra of (a) **L^{1}**, (b) **(HL^{1})$^{+}$Cl^{-}**, (c) **(HL^{1})$^{+}$Br^{-}**, (d) **[H(L^{1})$_{2}$]$^{+}$Br^{-}**, (e) **(HL^{1})$^{+}$NO$_{3}^{-}$**, (f) **(HL^{1})$^{+}$HSO$_{4}^{-}$**, (g) **(HL^{1})$_{2}^{2+}$SO$_{4}^{2-}$**, (h) **(HL^{2})$^{+}$Cl^{-}**, (i) **(HL^{2})$^{+}$Br^{-}**, (j) **HL^{2})$^{+}$NO$_{3}^{-}$** and (k) **(HL^{2})$^{+}$HSO$_{4}^{-}$**.

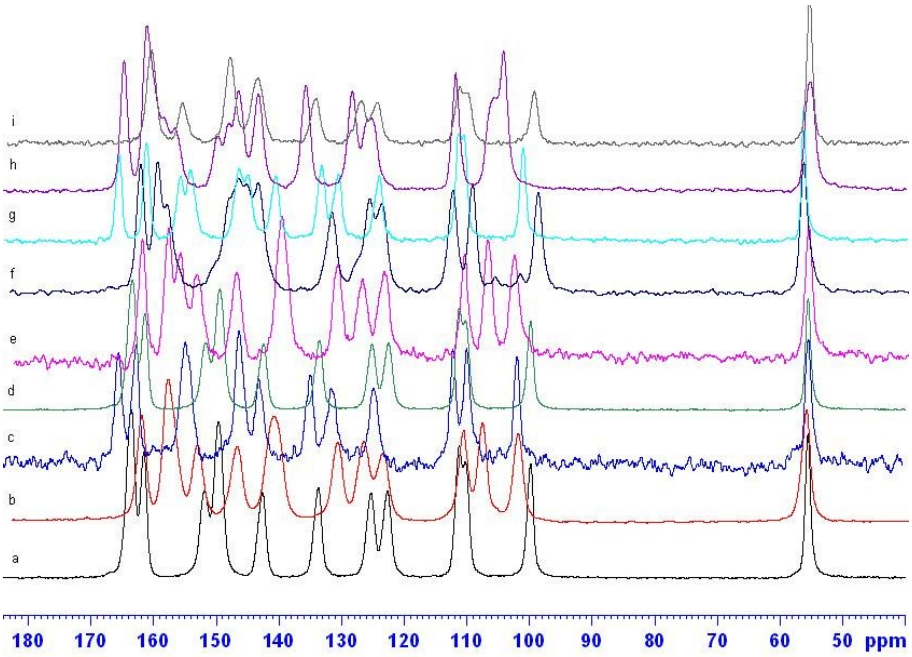

Figure S21. ^{13}C CP-MAS spectra of (a) **L^{1}**, (b) **(HL^{1})$^{+}$ Cl^{-}**, (c) **(HL^{1})$^{+}$Br^{-} (α)**, (d) **(HL^{1})$^{+}$Br^{-} (β)** (e) **[H(L^{1})$_{2}$]$^{+}$Br^{-}**, (f) **(HL^{1})$^{+}$NO$_{3}^{-}$**, (g) **(HL^{1})$^{+}$HSO$_{4}^{-}$ (α)**, (h) **(HL^{1})$_{2}^{2+}$SO$_{4}^{2-}$** and (i) **(HL^{1})$^{+}$HSO$_{4}^{-}$ (β)**.

6. *Biological activity*

Table S12. *In vitro* antimicrobial activity of hydrazones and corresponding salts against Gram-positive and Gram-negative antibiotic susceptible and resistant strains by disc diffusion assay

Comp.	**Inhibition zone diameter (mm)**						
	Gram-positive bacteria				**Gram-negative bacteria**		
	B. cereus	*C. perfringens*	*S. aureus*	*S. aureus* MRSA	*E. coli*	*K. pneumoniae*	*A. baumannii*
L^1	17.0 ± 1.7	10.0 ± 1.9	26.0 ± 0.6	24.0 ± 0.7	21.0 ± 1.7	14.0 ± 1.9	23.0 ± 0.6
$(HL^1)^+Cl^-$	15.7 ± 1.5	15.2 ± 1.4	15.2 ± 1.7	17.2 ± 1.3	15.7 ± 1.5	10.2 ± 1.4	20.2 ± 1.7
$(HL^1)^+Br^-$	16.4 ± 0.5	9.7 ± 1.2	18.5 ± 1.2	25.4 ± 0.2	17.4 ± 0.5	13.7 ± 1.2	15.5 ± 1.2
$(HL^1)^+NO_3^-$	15.6 ± 1.1	14.6 ± 0.9	15.4 ± 1.9	12.6 ± 0.9	12.6 ± 1.1	13.6 ± 0.9	17.4 ± 1.9
$(HL^1)^+HSO_4^-$	12.8 ± 2.2	16.8 ± 0.9	11.8 ± 2.3	11.8 ± 0.9	10.8 ± 2.2	14.8 ± 0.9	15.8 ± 2.3
L^2	16.8 ± 0.8	14.4 ± 1.7	12.8 ± 0.3	14.8 ± 0.9	17.8 ± 0.8	14.4 ± 1.7	18.2 ± 0.3
$(HL^2)^+Cl^-\cdot 0.5H_2O$	17.3 ± 1.1	12.3 ± 1.1	26.5 ± 1.1	26.3 ± 1.1	15.3 ± 1.1	17.3 ± 1.1	17.5 ± 1.1
$(HL^2)^+Br^-\cdot MeOH$	15.8 ± 1.3	16.6 ± 1.2	10.4 ± 0.7	12.8 ± 0.6	14.8 ± 1.3	16.6 ± 1.2	16.4 ± 0.7
$(HL^2)^+NO_3^-$	17.8 ± 1.0	12.8 ± 2.1	15.3 ± 1.8	25.3 ± 1.1	17.8 ± 1.0	17.7 ± 2.1	15.3 ± 1.8
$(HL^2)^+HSO_4^-$	20.0 ± 1.6	10.0 ± 1.8	10.0 ± 0.6	12.0 ± 0.7	11.0 ± 1.6	14.0 ± 1.8	11.0 ± 0.6
Gentamicin	25.3 ± 0.7	26.2 ± 2.5	21.2 ± 1.4	11.2 ± 1.3	25.3 ± 0.7	26.2 ± 2.5	14.2 ± 1.0
Cefotaxime	28.0 ± 1.7	27.0 ± 1.9	19.0 ± 0.6	13.0 ± 0.7	28.0 ± 1.7	27.0 ± 1.9	12.0 ± 0.9

Disc diffusion assay. In order to investigate the antimicrobial potential of the hydrazones and corresponding salts a disc diffusion assay was employed according to the CLSI guidelines. 100 μL of suspension containing 10^5 colony-forming units (cfu/mL) of bacterial cells strains was spread on a Luria–Bertani (LB) agar. The tested powders were suspended in dimethyl sulfoxide (DMSO) to prepare a stock solution of 10 mg/mL concentration.

The sterile filter discs (6 mm) were individually loaded with 25 μL of the stock solution equivalent to a final concentration at 250 μg/disc by synthesized compounds and then placed on the nutrient agar that had been previously inoculated with the target microbial strains. Additionally, DMSO was used as a negative control. Cefotaxime (30 μg/disc) and gentamicin (15 μg/disc) were used as positive controls. The plates were incubated for 24 h at 37 ^{o}C. Antibacterial activity was assessed by measuring the diameter of the inhibition zone in millimetres. Samples were assayed in triplicate for each condition and the diameter of inhibition zones were presented as mean ± SE values.

Minimum inhibitory concentration testing. In addition, antimicrobial activities of the hydrazones and corresponding salts were also tested by a broth microdilution assay in 96 well plates. The standard two fold serial microdilution assay described by the Clinical and Laboratory Standards Institute was performed for the assessment of the minimum inhibitory concentrations (MICs). Bacteria were grown overnight in Luria–Bertani (LB) broth at 37 °C. The microbial cultures were diluted in fresh LB broth to a final concentration of 10^6 CFU mL^{-1} for bacteria strains. The compounds were first dissolved in DMSO and incorporated into aqueous nutrient medium to obtain a concentration of 10 mg mL^{-1}. The stock solution was then serially two fold diluted to obtain concentrations ranging from 500 to 0.09 μg mL^{-1} in sterile plates containing LB broth. Serial dilutions of the compounds were added to the microtiter plates in a volume of 100 μL. Each well was additionally inoculated with 10 μL of

inoculums of the target microorganism and then incubated at 37 °C for 18-24 h. The MIC value was determined as the lowest concentration of the sample at which the tested microorganisms did not demonstrate any visible growth after incubation. As an indicator of bacterial growth. 50 μL of 0.2 mg mL^{-1} *p*-iodonitrotetrazolium chloride (INT; Sigma-Aldrich Co. Ltd. Poole. UK) was added to the wells and incubated at 37 °C for 30 min. Following addition of INT and incubation, the MIC was determined as the lowest sample concentration at which no pink color appeared. Cefotaxime and gentamicin were used as positive controls. Minimum inhibitory concentrations of the commercial antibiotics were determined by the E-test (AB Biodisk, Solna, Sweden).